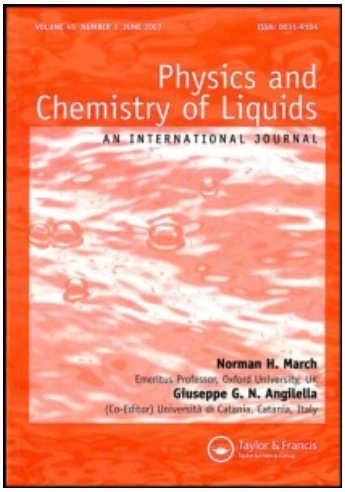

Physics and Chemistry of Liquids
Publication details, including instructions for authors and subscription information:
http://www.informaworld.com/smpp/title~content=t713646857

Effect of critical fluctuations on adsorption of van der Waals fluid in a spherical cavity

Yongyi Peng[a]; Hui Zou[a]; Yuantao Xiang[a]; Kechao Zhou[b]; Xiaobin Li[c]
[a] School of Physical Science and Technology, Central South University, Changsha 410083, P.R. China [b] Research Institute of Powder Metallurgy, Central South University, Changsha 410083, P.R. China [c] School of Metallurgical Science and Engineering, Central South University, Changsha 410083, P.R. China

Online publication date: 10 December 2010

To cite this Article Peng, Yongyi , Zou, Hui , Xiang, Yuantao , Zhou, Kechao and Li, Xiaobin(2010) 'Effect of critical fluctuations on adsorption of van der Waals fluid in a spherical cavity', Physics and Chemistry of Liquids, 48: 6, 810 — 827
To link to this Article: DOI: 10.1080/00319104.2010.489188
URL: http://dx.doi.org/10.1080/00319104.2010.489188

Physics and Chemistry of Liquids
Vol. 48, No. 6, December 2010, 810–827

Taylor & Francis
Taylor & Francis Group

Effect of critical fluctuations on adsorption of van der Waals fluid in a spherical cavity

Yongyi Peng[a]*, Hui Zou[a], Yuantao Xiang[a], Kechao Zhou[b] and Xiaobin Li[c]

[a]*School of Physical Science and Technology, Central South University, Changsha 410083, P.R. China;* [b]*Research Institute of Powder Metallurgy, Central South University, Changsha 410083, P.R. China;* [c]*School of Metallurgical Science and Engineering, Central South University, Changsha 410083, P.R. China*

(*Received 1 February 2010; final version received 24 April 2010*)

A recently proposed non-uniform fifth-order thermodynamic perturbation theory (TPT) is employed to investigate the adsorption of a hard core attractive Yukawa (HCAY) fluid in a spherical cavity. Extensive comparison with available simulation data indicate that the non-uniform fifth-order TPT is sufficiently reliable in calculating the density profiles of the HCAY fluid in the highly confining geometry, and generally is more accurate than a previous third-order + second-order perturbation density functional theory. The non-uniform fifth-order TPT is free from numerically solving an Ornstein–Zernike integral equation, and also free of any adjustable parameter; consequently, it can be applied to both supercritical and subcritical temperature regions. The non-uniform fifth-order TPT is employed to investigate critical adsorption of the HCYA fluid in a single spherical cavity – it is disclosed that the critical fluctuations near the critical point induce depletion adsorption – quantitative theoretical calculation on relationship between the critical depletion adsorption, parameters of coexistence bulk phase and the responsible external field is in agreement with qualitative physical analysis.

Keywords: liquids; adsorption; thermodynamic perturbation theory

1. Introduction

Adsorption is a very important chemical engineering operational unit, which plays key roles in many phenomena, such as catalysis, separation, crystallisation from solution and phase transitions in confining geometries, such as capillary condensation, layering and wetting transitions of fluids in pores [1]. In recent years, theoretical description of adsorption phenomena is largely based on a so-called non-local density functional theory (NDFT) [1] whose significant improvement over a local density functional theory (LDFT) [1] lies in that the NDFT can satisfactorily describe the structure of simple confined fluids, namely an oscillatory density profile near solid surfaces or of fluids in confining geometries, such as slits, cylinders and spheres. From the point of view of a theoretical formalism, all of the published NDFTs can be categorised into different types according to their treatment ways for an attractive part of the underlying interaction potential. In the NDFTs reported in

*Corresponding author. Email: yongyip@163.com

ISSN 0031–9104 print/ISSN 1029–0451 online

DOI: 10.1080/00319104.2010.489188
http://www.informaworld.com

Ref. [2], the attractive part is treated on the level of a van der Waals theory for the simple bulk fluids, the uniform limit of the NDFT [2] is exactly equivalent to the van der Waals treatment on the attractive part of the potentials. For these NDFT approaches, the only input is a hard sphere density functional approximation (DFA), which is employed to treat the hard sphere repulsion part of the potential. Several existing hard sphere DFAs can serve well for the aim: weighted density approximation (WDA) due to Tarazona [3a], and Curtin and Ashcroft [3b], a well-known variant of the WDA, i.e. fundamental measure functional (FMF) due to Rosenfeld [4a] and Kierlik and Rosinberg [4b], a Lagrangian theorem-based density functional approximation (LTDFA) [5a] and its adjustable parameter free version [5b] and finally a so-called bridge DFA [6]. Since there is no need for a bulk second-order direct correlation function (DCF) as input, the NDFT reported in Ref. [2] can conveniently treat the subcritical adsorption phenomena [1,2,7], such as capillary condensation and wetting transitions of fluids in pores and depict the phase diagram of fluids in confining conditions. The drawback of this kind of NDFT [2] is that the prediction accuracy for the density profile is unsatisfactory, which arises from an oversimplified treatment on the attractive part of the potential. In the NDFTs [8], both the attractive part and the hard sphere repulsion part are treated on the same level by the WDAs, and the weighting function is obtained by solving an integral-differentiation equation involving the bulk second-order DCF over a density range. Therefore, the numerical implementation of this kind of NDFT [8] needs the bulk second-order DCF over a density range as input, this makes this kind of NDFT [8] unable to treat the subcritical adsorption phenomena of the van der Waals fluids. In the NDFT reported in Ref. [9], the bulk second-order DCF is divided into a hard core part and a tail part, it is thought that the tail part can be sufficiently treated on the level of the second-order perturbation expansion, whereas the hard core part has to be treated by higher order perturbation expansion approximations or by other efficient hard sphere DFAs. This kind of NDFT [9a,10,11] only requires the second-order DCF of the coexistence bulk fluid as input, therefore it can be used to investigate the subcritical adsorption phenomena. In fact, this kind of NDFT [10] is presently the most accurate density functional theory (DFT) version for the van der Waals fluids. The only drawback of the NDFT [10] is that one has to determine an associated physical parameter beforehand. In the NDFT, reported in Ref. [12], the hard core repulsion and the attractive tail are treated separately by different WDAs. The NDFTs by Sweatman [13a], and by Kim and Lee [13b] employ the bulk seco nd-order DCF as input from numerical solution of the Ornstein–Zernike (OZ) integral equation theory (IET) for calculation of weighting function needed to calculate the involved weighted densities, their application to subcritical adsorption is either involved with very complicated mathematical process [13a] or is impossible at all [13a, b]. Obviously an NDFT, which is free of the numerical bulk seco nd-order DCF and any adjustable physical parameter, but can be applied with satisfactory accuracy to both the supercritical and subcritical regions, is very desirable. It is noted that a recent literature [14d] achieves this goal, the formalism in Ref. [14d] is based on a recently proposed fifth-order thermodynamic perturbation theory (TPT) [14d], which is actually a higher order version of a recently proposed coupling parameter expansion TPT [14a–c], but the fifth-order TPT [14d] is extended in Ref. [14d] from bulk to non-uniform situation in the framework of classical DFT. The aim of this study is twofold. Firstly, the recent non-uniform fifth-order TPT [14d] is tested in a

harsh situation, i.e. adsorption of a hard core attractive Yukawa (HCAY) fluid in a single spherical cavity; secondly, we employ the non-uniform fifth-order TPT to investigate influence of the critical fluctuations on the adsorption of the HCAY fluid in the single spherical cavity.

Organisation of this article is as follows. In Section 2, the formalism of the non-uniform fifth-order TPT [14d] is briefly recounted and is applied to the HCAY fluid confined in a single spherical cavity, the resultant theoretical calculations for the density profiles are compared with the corresponding simulation data available in literature; it also will be shown that the non-uniform fifth-order TPT can predict very accurately a radial distribution function (rdf) of the bulk HCAY fluid. In Section 3, we apply the non-uniform fifth-order TPT [14d] to the near critical and supercritical adsorption of the HCAY fluid in a single spherical cavity and explore the influence of the critical fluctuations on the adsorption behaviour. Finally, in Section 4, this research is concluded.

2. Non-uniform fifth-order TPT

In the non-uniform fifth-order TPT [14d], bulk excess Helmholtz free energy $F_{ex}(\rho_b)$ for a system of N particles in a volume V interacting via a full pair potential $u(r)$ is employed as input to construct the corresponding non-uniform $F_{ex}[\rho(\mathbf{r})]$ to be used in the framework of the classical DFT. $F_{ex}(\rho_b)$ is calculated by a recently proposed TPT based on the coupling parameter expansion; when the series is truncated at $n=3$, the resultant third-order TPT [14a–c] is shown to be a large improvement over a traditional second-order macroscopic compressibility approximation (MCA) [16] TPT; while, when the series is truncated at $n=5$, the resultant fifth-order TPT [14d] is also shown to be an improvement over the third-order TPT [14a–c]. In this article, the fifth-order version of the coupling parameter expansion TPT will be employed; detail of relevant numerical implementation can be referred to [14].

In the classical DFT, the equilibrium density profile $\rho(\mathbf{r})$ is calculated by an Euler–Lagrange equation resulting from minimisation of an approximate grand potential functional

$$\rho(\mathbf{r}) = \rho_b \exp\{-\beta\varphi_{ext}(\mathbf{r}) + C^{(1)}(\mathbf{r};[\rho]) - C_0^{(1)}(\rho_b)\}, \tag{1}$$

where $C^{(1)}(\mathbf{r};[\rho])$ is the first-order DCF of the non-uniform fluid, $C_0^{(1)}(\rho_b)$ the uniform first-order DCF of the corresponding coexistence bulk fluid of density ρ_b.

$C^{(1)}(\mathbf{r};[\rho])$ is mathematically first-order functional derivative of $F_{ex}[\rho(\mathbf{r})]$ with respect to $\rho(\mathbf{r})$

$$C^{(1)}(\mathbf{r};[\rho]) = \frac{-\delta\beta F_{ex}[\rho]}{\delta\rho(\mathbf{r})}. \tag{2}$$

In Refs. [9,10] $C^{(1)}(\mathbf{r};[\rho])$ and $F_{ex}[\rho(\mathbf{r})]$ are divided into hard core part and tail part

$$F_{ex}[\rho(\mathbf{r})] = F_{ex-hc}[\rho(\mathbf{r})] + F_{ex-tail}[\rho(\mathbf{r})] \tag{3}$$

$$C^{(1)}(\mathbf{r};[\rho]) = C_{hc}^{(1)}(\mathbf{r};[\rho]) + C_{tail}^{(1)}(\mathbf{r};[\rho]); \tag{4}$$

correspondingly, one has:

$$F_{ex}(\rho_b) = F_{ex-hc}(\rho_b) + F_{ex-tail}(\rho_b) \tag{5}$$

$$C_0^{(1)}(\rho_b) = C_{0-\mathrm{hc}}^{(1)}(\rho_b) + C_{0-\mathrm{tail}}^{(1)}(\rho_b) \tag{6}$$

and consequently

$$C^{(1)}(\mathbf{r};[\rho]) - C_0^{(1)}(\rho_b) = [C_{\mathrm{hc}}^{(1)}(\mathbf{r};[\rho]) - C_{0-\mathrm{hc}}^{(1)}(\rho_b)] + \left[C_{\mathrm{tail}}^{(1)}(\mathbf{r};[\rho]) - C_{0-\mathrm{tail}}^{(1)}(\rho_b)\right]. \tag{7}$$

Considering that $F_{\mathrm{ex}}(\rho_b)$ from the fifth-order TPT is employed in Ref. [14d] as input, one can assume self-consistently $F_{\mathrm{ex-hc}}(\rho_b) = F_{\mathrm{ex-ref}}(\rho_b)$. As for the treatment for $F_{\mathrm{ex-hc}}[\rho(\mathbf{r})]$, the non-uniform fifth-order TPT employs the LTDFA [5], therefore, one has

$$C_{\mathrm{hc}}^{(1)}(\mathbf{r};[\rho]) - C_{0-\mathrm{hc}}^{(1)}(\rho_b) = \int \mathrm{d}\mathbf{r}_1(\rho(\mathbf{r}_1) - \rho_b)C_{0-\mathrm{hs-PY}}^{(2)}(|\mathbf{r}-\mathbf{r}_1|;\tilde{\rho}_{\mathrm{hc}}((\mathbf{r}+\mathbf{r}_1)/2,\lambda)), \tag{8}$$

where the hard core weighted density $\tilde{\rho}_{\mathrm{hc}}$ is given by

$$\tilde{\rho}_{\mathrm{hc}}((\mathbf{r}+\mathbf{r}_1)/2,\lambda) = \int \mathrm{d}\mathbf{r}' C_{0-\mathrm{hs-PY}}^{(2)}\left(|(\mathbf{r}+\mathbf{r}_1)/2-\mathbf{r}'|;\rho_b\right)[\rho_b + \lambda(\rho(\mathbf{r}')-\rho_b)]/C_{0-hs-PY}^{(1)\prime}(\rho_b). \tag{9}$$

In Equations (8) and (9), $C_{0-\mathrm{hs-PY}}^{(n)}$ is a bulk hard sphere fluid nth-order DCF, $C_{0-\mathrm{hs}}^{(1)\prime}(\rho_b)$ stands for first-order derivative of the bulk hard sphere fluid first-order DCF with respect to the density argument ρ_b. The subscript PY means that the $C_{0-\mathrm{hs-PY}}^{(n)}$ and $C_{0-\mathrm{hs-PY}}^{(1)\prime}(\rho_b)$ are obtained under Percus–Yevick approximation [17] for the OZ IET. Regarding the numerical value of the parameter λ, we will discuss it later in this study.

As for $C_{\mathrm{tail}}^{(1)}(\mathbf{r};[\rho])$, Ref. [14a, d and h] propose using the following approximation [1] for $F_{\mathrm{ex-tail}}[\rho(\mathbf{r})]$:

$$F_{\mathrm{ex-tail}}[\rho(\mathbf{r})] = \int \mathrm{d}\mathbf{r}\rho(\mathbf{r}) f_{\mathrm{ex-tail}}(\tilde{\rho}_{\mathrm{tail}}(\mathbf{r})) \tag{10}$$

where $f_{\mathrm{ex-tail}}$ is the bulk excess Helmholtz free energy per particle for the tail part. Considering that one has assumed $F_{\mathrm{ex-hc}}(\rho_b) = F_{\mathrm{ex-ref}}(\rho_b)$, therefore, we have [14d]

$$f_{\mathrm{ex-tail}}(\rho_b) = F_{\mathrm{ex-tail}}(\rho_b)/N = (F_{\mathrm{ex}}(\rho_b) - F_{\mathrm{ex-ref}}(\rho_b))/N. \tag{11}$$

The weighted density $\tilde{\rho}_{\mathrm{tail}}(\mathbf{r})$ is calculated by a simple WDA [18],

$$\tilde{\rho}_{\mathrm{tail}}(\mathbf{r}) = \int \rho(\mathbf{r}')w(|\mathbf{r}-\mathbf{r}'|;\rho_b) \tag{12}$$

$$w(\mathbf{r};\rho_b) = C_{0-\mathrm{tail}}^{(2)}(\mathbf{r};\rho_b) \Big/ \int \mathrm{d}\mathbf{r} C_{0-\mathrm{tail}}^{(2)}(\mathbf{r};\rho_b). \tag{13}$$

$C_{0-\mathrm{tail}}^{(2)}(\mathbf{r};\rho_b)$ is a tail part of the bulk second-order DCF $C_0^{(2)}(\mathbf{r};\rho_b)$ for the full pair potential $u(r)$. In parallel with Equation (2), one has

$$\begin{aligned} C_{\mathrm{tail}}^{(1)}(\mathbf{r};[\rho]) &= \frac{-\delta\beta F_{\mathrm{ex-tail}}[\rho]}{\delta\rho(\mathbf{r})} \\ &= -\beta f_{\mathrm{ex-tail}}(\tilde{\rho}_{\mathrm{tail}}(\mathbf{r})) - \int \mathrm{d}\mathbf{r}'\rho(\mathbf{r}')\beta f'_{\mathrm{ex-tail}}(\tilde{\rho}_{\mathrm{tail}}(\mathbf{r}'))w(|\mathbf{r}-\mathbf{r}'|;\rho_b). \end{aligned} \tag{14}$$

After taking the limit of $\rho(\mathbf{r}) \to \rho_b$ on $C^{(1)}_{\text{tail}}(\mathbf{r};[\rho])$, one obtains $C^{(1)}_{0-\text{tail}}(\rho_b)$. The above derivation directly leads to a numerically tractable density profile equation,

$$\begin{aligned}\rho(\mathbf{r}) = \rho_b \exp\{&-\beta\varphi_{\text{ext}}(\mathbf{r}) + \int d\mathbf{r}_1(\rho(\mathbf{r}_1) - \rho_b)C^{(2)}_0(|\mathbf{r}-\mathbf{r}_1|;\tilde{\rho}_{\text{hc}}((\mathbf{r}+\mathbf{r}_1)/2,\lambda)) \\ &- \beta f_{\text{ex}-\text{tail}}(\tilde{\rho}_{\text{tail}}(\mathbf{r})) - \int d\mathbf{r}'\rho(\mathbf{r}')\beta f'_{\text{ex}-\text{tail}}(\tilde{\rho}_{\text{tail}}(\mathbf{r}'))w(|\mathbf{r}-\mathbf{r}'|;\rho_b) \\ &+ \beta f_{\text{ex}-\text{tail}}(\rho_b) + \beta\rho_b f'_{\text{ex}-\text{tail}}(\rho_b)\}. \end{aligned} \tag{15}$$

In Ref. [14d], three principles are proposed for guiding in choosing approximation for $C^{(2)}_{0-\text{tail}}(\mathbf{r};\rho_b)$, the resultant approximation for $C^{(2)}_{0-\text{tail}}(\mathbf{r};\rho_b)$ is given

$$\begin{array}{ll} C^{(2)}_{0-\text{tail}}(\mathbf{r};\rho_b) = (\chi_p - 1)C^{(2)}_{0-\text{hs}-\text{PY}}(\mathbf{r};\rho_b) & r < \sigma \\ \exp(-\beta u(\mathbf{r})) - 1 & r \geq \sigma. \end{array} \tag{16}$$

Here,

$$\begin{array}{ll} \chi_p = \chi & \chi \leq 1 \\ 1 & \chi > 1. \end{array} \tag{17}$$

As for specification of the parameter χ, one can determine it by thermodynamic self-consistency condition given by

$$1 - \rho_b \int d\mathbf{r} C^{(2)}_0(\mathbf{r};\rho_b) = 1/\chi_T = (\partial\beta P/\partial\rho_b)_T, \tag{18}$$

where $(\partial\beta P/\partial\rho_b)_T$ can be calculated by the employed uniform fifth-order TPT.

When we employ the adjustable parameter free version [5b] of the hard sphere LTDFA [5a] for use as the approximation of the hard core part, i.e. the physical parameter; λ in Equations (8, 9) is set to be 0.5, the resultant predictions for the density profile of the HCAY fluid as simulated in Ref. [19] deviate sometimes largely from the simulation results. Considering that the hard sphere LTDFA [5a] holds a self-correction efficacy [20], which can make good the likely un-appropriateness of an approximate bulk second-order DCF as input, and ensure the final theoretical results are still satisfactory, we suggest to use the LTDFA [5a] instead of its adjustable parameter free version [5b]. Then, how to specify the physical parameter λ constitutes a new problem. Determination of the λ by the so-called hard wall sum rule [21] is certainly a way; however, this way will incur inconvenience in application as one has to determine beforehand the value of λ for every coexistence bulk condition. Unlike the case in Ref. [20], where the numerical value of λ changes drastically when the bulk coexistence conditions change, for the present case, λ remains near a fixed value, the value is about 0.45. The fortunate phenomenon has its physical origin, which will be explained as follows. Unlike the case in Ref. [20], where the reliability of the bulk second-order DCF for the polymer from solving numerically a polymer-RISM integral equation varies obviously as the bulk parameters change, therefore the dependence on self-correction efficacy of the LTDFA [5a] also changes drastically, this leads to a very dispersing numerical value of λ. In this case, the performance of the ansatz bulk second-order DCF is stable due to the imposition of the thermodynamic self-consistency condition, the shifting of λ value from the original 0.5 to the present 0.45 only helps to offset the systematical

error incurred by the ansatzs for the bulk second-order DCF. This explanation is furthermore evidenced by the observation disclosed in Ref. [22], where it is shown that λ still remains at 0.5 when the polymer-reference interaction site model (RISM) bulk second-order DCF is scaled by a coefficient, which is determined by the polymer equation of state combined with the isothermal compressibility equation. By adjusting the present λ value to a fixed value of 0.45, the present inaccuracy for the density profile is largely lowered. From this observation, one can draw two remarks. One is that the error originating from the ansatzs for the bulk second-order DCF is systematical, therefore a constant lowering of λ value, which can lead to a whole shifting of the density profile as shown by $\rho_b + \lambda(\rho(\mathbf{r}) - \rho_b)$ in Equation (13), repair well the approximation of the ansatzs; the other is that the validity of $\lambda = 0.45$ fully demonstrates the self-correction efficacy of the LTDFA [5a] as explained in detail in Ref. [20]. Throughout the study, the value of λ is fixed at 0.45.

We will test the accuracy of the non-uniform fifth-order TPT for calculating the density distribution of the HCAY fluid being subjected to an external potential due to a highly confining geometry, i.e. a spherical cavity and maintaining equilibrium with the bulk fluid, when the latter is in the state of (1) supercritical temperature but close to the critical value with the density ranging from low to high density region and (2) subcritical temperature with the density near the liquid–vapour coexistence line.

The external potential due to a hard spherical cavity is given by

$$\begin{aligned} \phi_{\text{ext}}(\mathbf{r}) &= 0 \quad |\mathbf{r}| < R \\ &= \propto \quad |\mathbf{r}| > R. \end{aligned} \tag{19}$$

When the external field is due to a bulk HCAY particle situated at the origin, the external potential is given by

$$\varphi_{\text{ext}}(\mathbf{r}) = u_{\text{HCAY}}(r), \tag{20}$$

where $u_{\text{HCAY}}(r)$ is the interaction potential between two HCAY particles separated by an interval r,

$$\begin{aligned} u_{\text{HCAY}}(r) &= \propto \quad r/\sigma < 1 \\ &= -\varepsilon\sigma \exp[-\kappa^*(r-\sigma)/\sigma]/r \quad r/\sigma > 1, \end{aligned} \tag{21}$$

where ε is an interaction strength and κ^* a reduced potential range parameter. For the case of the external potential Equation (20), the reduced density distribution function $\rho(\mathbf{r})/\rho_b$ is actually the bulk rdf $g(\mathbf{r})$ according to the Percus' test particle method [23].

The computer simulation bulk phase behaviour of the HCAY fluid is given in Ref. [24], this helps the choice of the coexistence bulk fluid parameters in this article and in Ref. [19]. The present theoretical predictions for the density profiles are presented in Figures (1–4) together with the corresponding simulation results available in Ref. [19]. Throughout the text, a reduced temperature is defined as $T^* = kT/\varepsilon$ with k being Boltzmann constant and T absolute temperature.

Now, we will give a detailed comparison of the present Figures (1–4) with figures (16–19) in Ref. [19], where the theoretical predictions are based on a third-order + second-order perturbation DFT [9a,19]. We have not presented the

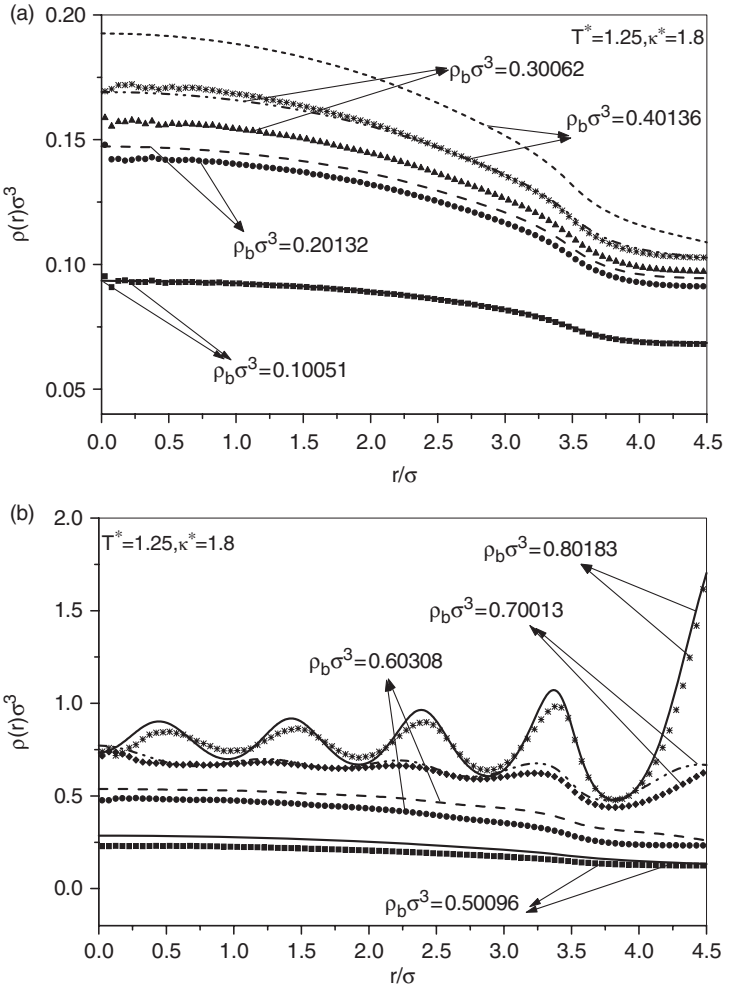

Figure 1. The present theoretical (lines) and simulation (symbols) results for the density profiles of the HCAY fluid in a spherical cavity of radius $R = 4.5\sigma$ at supercritical temperature for the chosen potential range parameter. Notes: The coexistence of bulk densities and potential range parameter chosen are shown in the figure; the simulation results are reproduced from [19].

third-order + second-order perturbation DFT predictions in Figures (1–4) only to make the figures clear enough since each one of the Figures (1–4) presents several curves corresponding to different coexistence bulk densities.

A comparison between the present Figures (1–4) and the Figures (16–19) of Ref. [19] discloses that the third-order + second-order perturbation DFT is a little more accurate than the non-uniform fifth-order TPT–ZDL–PTS for the parameter combination of $\kappa^* = 1.8$ and $T^* = 1.25$ except for the cases of the two highest coexistence bulk densities where the present approach is more accurate than the third-order + second-order perturbation DFT. For the parameter combinations of $\kappa^* = 3.0$, $T^* = 0.76$ and $\kappa^* = 4.0$, $T^* = 0.61$, the present approach is obviously more accurate than the third-order + second-order perturbation DFT, but both the

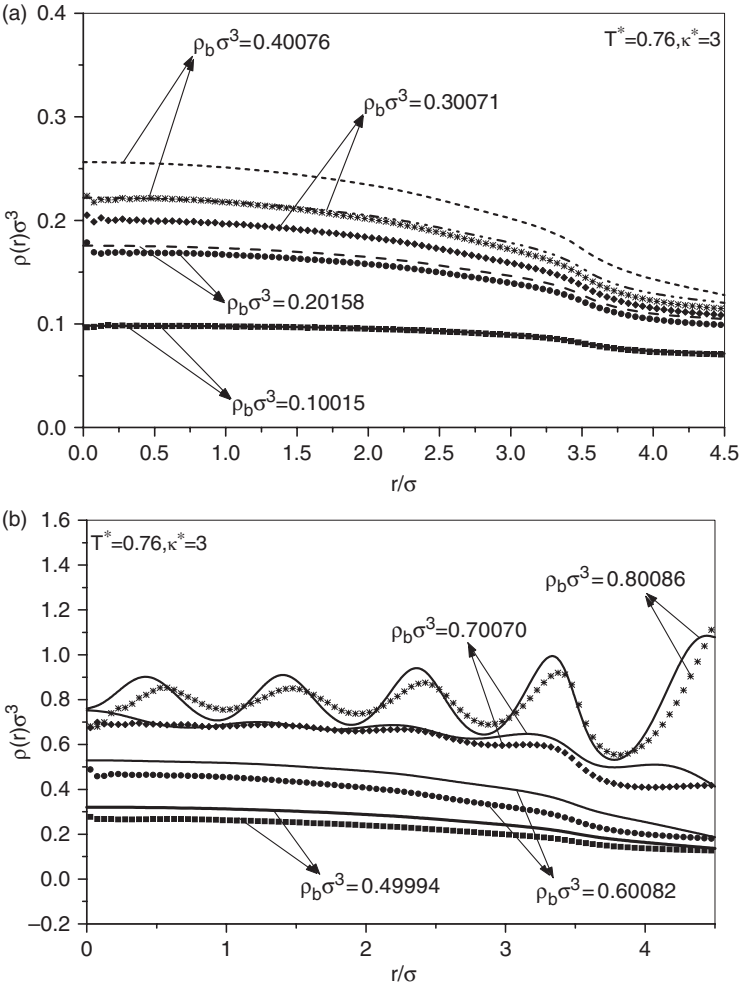

Figure 2. Same as Figure 1 but for the coexistence of bulk densities, potential range parameter and temperature as shown in the figure.

approaches become more inaccurate when the coexistence bulk densities increase. For the subcritical temperature cases, the present approach performs better than the third-order + second-order perturbation DFT.

For the external field due to a HCAY particle denoted by Equations (20) and (21), the two approaches behave well for the calculation of the rdf $g(\mathbf{r})$. However, it is still easy to observe the higher accuracy of the present approach than that of the third-order + second-order perturbation DFT; for reason of page limit, the results are not presented.

To conclude, the non-uniform fifth-order TPT is generally more accurate than the third-order + second-order perturbation DFT. Concretely speaking, as the potential range becomes shorter, the present approach becomes more and more accurate than the third-order + second-order perturbation DFT. For a combination of the long potential range such as $\kappa^* = 1.8$ and a single hard wall external field as

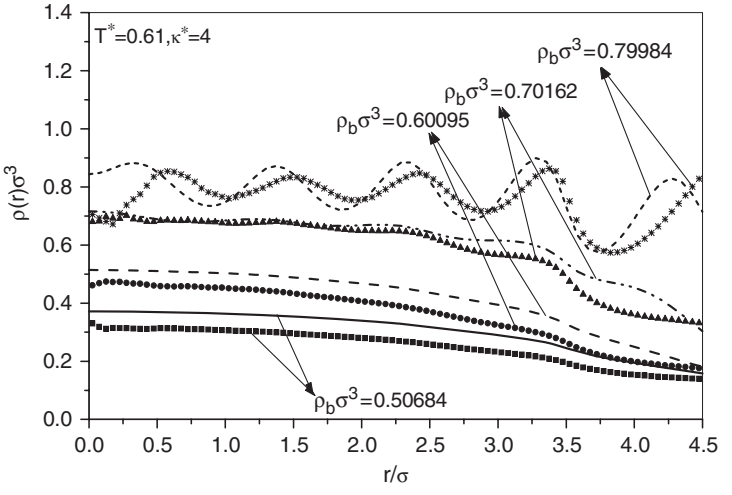

Figure 3. Same as Figure 1 but for the coexistence of bulk densities, potential range parameter and temperature as shown in the figure.

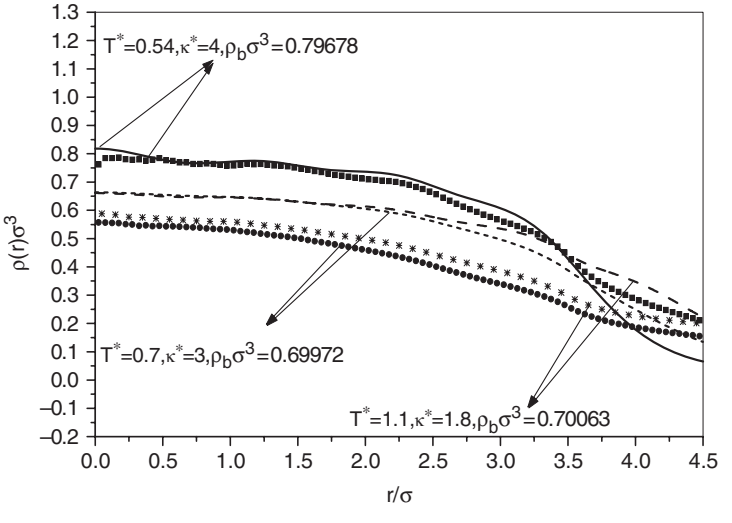

Figure 4. The present theoretical (lines) and simulation (symbols) results for the density profiles of the HCAY fluid in a spherical cavity of radius $R = 4.5\sigma$ at subcritical temperature for each potential range parameter value chosen. Notes: The coexistence of bulk densities is at monophasic liquid state. The simulation results are reproduced from [19].

investigated in Refs. [9a, 19], extensive calculation and comparison indicate (due to page limit, the corresponding comparison is not presented) that on average the third-order + second-order perturbation DFT is not too inferior to the non-uniform fifth-order TPT, but for other external fields, the third-order + second-order perturbation DFT deteriorates drastically even the potential range is still fixed at $\kappa^* = 1.8$. As the satisfactory performance of the third-order + second-order perturbation DFT for the parameter combination of $\kappa^* = 1.8$ and the single hard wall cannot go on for other

external fields, one has reason to conclude that the satisfactory performance for this particular case originates from the adjustable parameter in the third-order + second-order perturbation DFT. In fact, succedent literatures [25] had indicated that the third-order + second-order formalism is physically reliable, it is the poor accuracy of the mean spherical approximation (MSA) bulk second-order DCF employed in Refs. [9a,19] that leads to unsatisfactory prediction accuracy for these harsh near critical phenomena. This observation only brings out the superiority of the present ansatzs bulk second-order DCF to the MSA bulk second-order DCF. The ansatzs bulk second-order DCF is free from solving numerically the OZ integral equation, and therefore, its application is not limited to several simple model potentials for which analytical bulk second-order DCFs are available in literature. Obviously, the satisfactory performance of the present bulk second-order DCF comes from the imposition of the thermodynamic self-consistency and a satisfactory accuracy of the employed uniform fifth-order TPT. It should be pointed out that the sample coexistence bulk states are near the critical point or near the gas–liquid coexistence lines, therefore the present test is harsh. Absence of any adjustable parameter from the present formalism makes the approach very convenient for application investigation and eligible for theoretical investigation, which needs intensive calculations.

It is interesting to compare the present non-uniform fifth-order TPT with an existing density functional approach by Tang and Wu (TW) [26]. In the TW approach, the hard core part is treated by the FMF [4a], the tail part is treated by the second-order functional perturbation expansion approximation. The key input, i.e. the tail part $C^{(2)}_{0-\mathrm{tail}}(r;\rho_b)$ of the bulk second-order DCF $C^{(2)}_0(r;\rho_b)$, is simply equal to the $C^{(2)}_0(r;\rho_b)$ for $r \geq d$ (d is being the effective hard sphere diameter), and zero for $r < d$. As for $C^{(2)}_0(r;\rho_b)$ itself, they obtain it by mapping the considered Lennard–Jones (LJ) potential onto a two Yukawa potential, which is solved analytically under the first-order MSA for the OZ integral equation. Obviously, the accuracy of TW approach depends on both the rationality of the mapping procedure and the reliability of the first-order MSA. Particularly, when the considered interaction potentials are wanting in an analytical first-order MSA solution, one has to numerically solve the OZ integral equation. On the other hand, the present formalism is free from any analytical or numerical solution of the OZ IET, it also does not involve any mapping procedure. Therefore, one can expect that the present formalism is applicable to a wide range of the potential functions.

3. Critical adsorption in spherical cavity

To investigate the critical adsorption of the HCAY fluid, we will use the spherical cavity as the sample of external field since the spherical cavity exerts the strongest confinement on the fluid particles among all of the usually investigated external fields. To describe quantitatively the adsorption, first we define the reduced excess adsorption Γ^*_{ex},

$$\Gamma^*_{\mathrm{ex}} = \sigma^2 \int_0^R [\rho(\mathbf{r}) - \rho_b] \mathrm{d}\mathbf{r}/(4\pi R^2). \tag{22}$$

The sample external field is given by

$$\begin{aligned}\varphi_{\text{ext}}(\mathbf{r}) &= \propto \quad |\mathbf{r}| > R \\ &= \varepsilon_{\text{ext}} \exp[\kappa^*_{\text{ext}}(r - R)] \quad |\mathbf{r}| < R. \end{aligned} \tag{23}$$

In Figures (5–12), Γ^*_{ex} of the HCAY fluid in the spherical cavity is presented for various coexistence bulk phase and external field parameter combinations, the chosen potential range parameter κ^* is, respectively, 1.8, 3 and 4. For these values of κ^*, the reduced critical temperature and critical density calculated by the uniform fifth-order TPT are, respectively, 1.235 and 0.31, 0.74 and 0.39, and 0.59 and 0.3954.

Figures (5–12) clearly show that when the coexistence bulk states are near the critical point, Γ^*_{ex} reaches a minimum, particularly Γ^*_{ex} is a large negative value. We call the maximum negative value of Γ^*_{ex} as 'critical depletion adsorption'. To explain physically the critical depletion adsorption and its relationship with the external field parameters and bulk parameters, we propose that the depletion or its counterpart, i.e. 'accumulation' in a confining geometrical body depends on three factors. Hard core repulsion induces accumulation of the fluid particles adjacent to the hard solid surface since the fluid particle can avoid the repulsion interaction, which can be experienced to the full extent in the bulk phase when they move adjacent to the solid surface. On the contrary, the attractive tail of the underlying potential can induce depletion of the fluid particles away from the hard solid surface since the fluid particle can enjoy the attractive interaction to the full extent in the bulk phase. Obviously, the accumulation adjacent to the solid surface can be strengthened by a high density, but the depletion away from the solid surface can be strengthened by a low density due to the fact that when the bulk density is high enough the repulsion

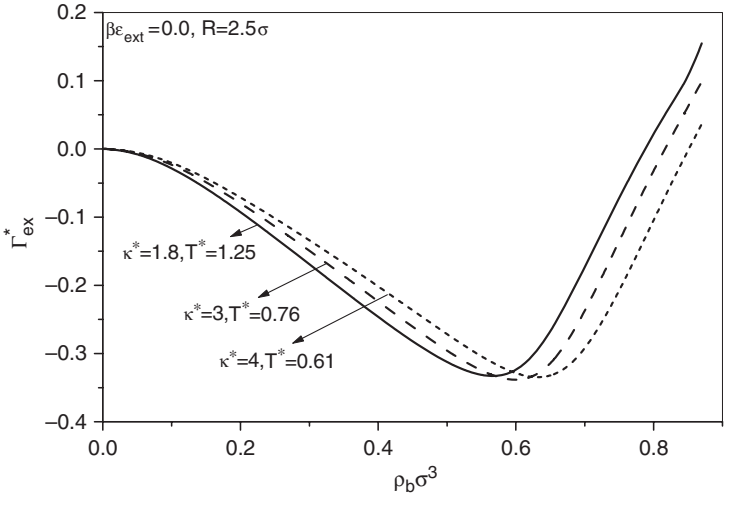

Figure 5. The excess adsorption Γ^*_{ex} as a function of reduced density $\rho_b\sigma^3$ for the HCAY fluid confined in a hard spherical cavity of radius $R = 2.5\sigma$. Notes: Reduced temperatures of the coexistence bulk phases are, respectively, very near respective critical reduced temperatures. The potential range parameters are, respectively, long-ranged ($\kappa^* = 1.8$) and intermediate-ranged ($\kappa^* = 3$ and $\kappa^* = 4$).

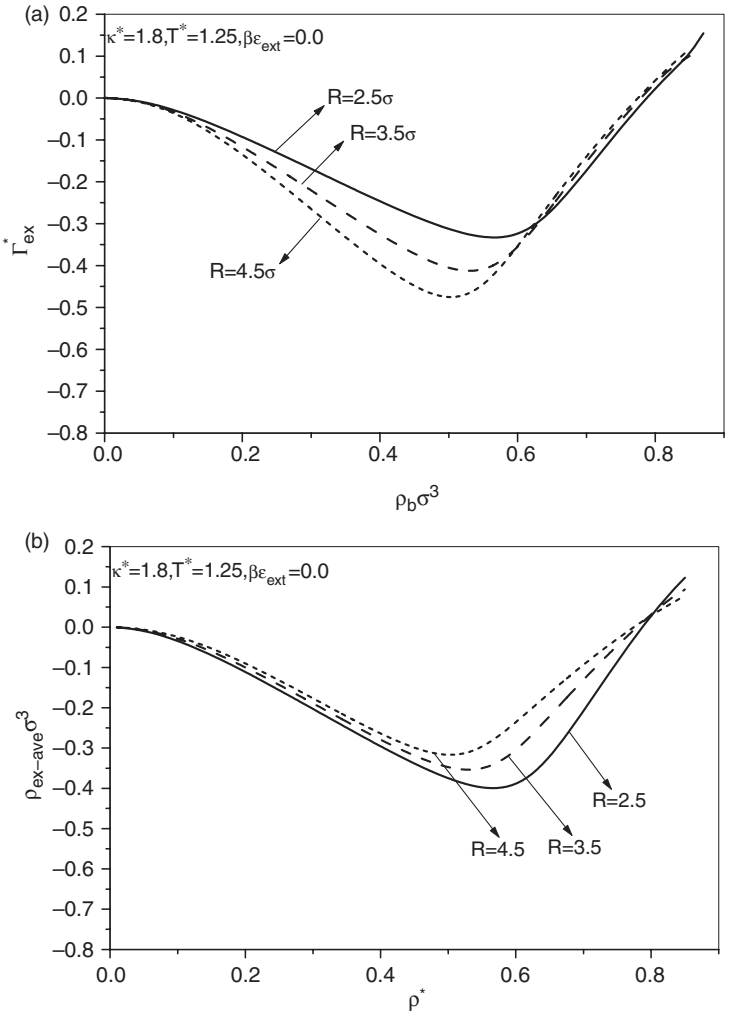

Figure 6. (a) The excess adsorption Γ^*_{ex} as a function of reduced density $\rho_b\sigma^3$ for the HCAY fluid ($\kappa^* = 1.8$ and $T^* = 1.25$) confined in a hard spherical cavity of radius $R = 2.5\sigma$, 3.5σ, 4.5σ, respectively; (b) The same as in figure a except that Γ^*_{ex} is substituted by the reduced excess average density $\rho_{ex-ave}\sigma^3$.

interaction in the bulk phase will play more and more important role, which makes the bulk environment unfavourable and the surface environment favourable. However, the high density-restraining depletion effect occurs only when the density is high enough. When the density is not high enough, an increasing density strengthens the depletion adsorption instead of restraining the depletion adsorption since more particles confined within a small space is an energetically unfavourable configuration. For the attractive tail-induced depletion, the influencing factors additionally include the critical fluctuation effect. Around the critical point, the correlation length unusually increases, when the geometrical size is smaller than the correlation length, the fluid particles will move out of the cavity to be situated in

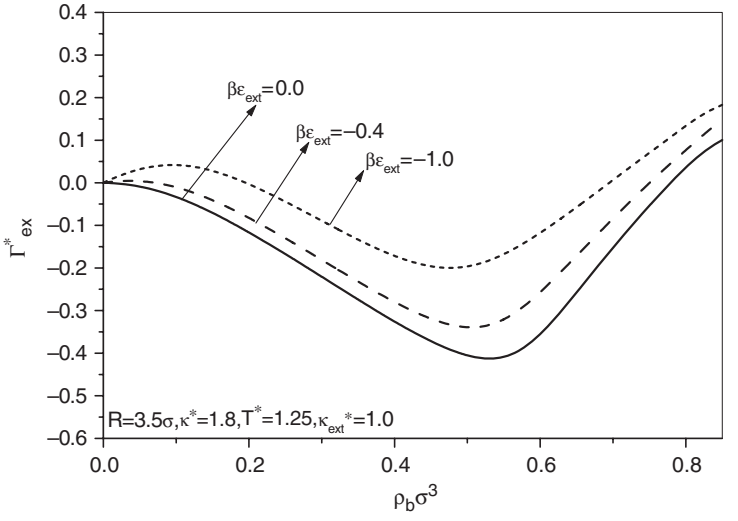

Figure 7. The excess adsorption Γ^*_{ex} as a function of reduced density $\rho_b\sigma^3$ for the HCAY fluid ($\kappa^* = 1.8$ and $T^* = 1.25$) confined in an attractive spherical cavity of radius $R = 3.5\sigma$. The external potential parameters are shown in the figure.

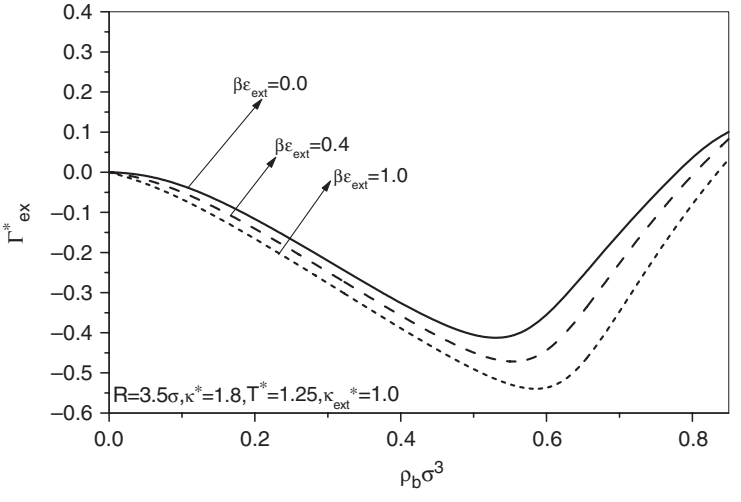

Figure 8. Same as in Figure 7 but the external potential is repulsive.

the bulk to enjoy to the full extent the attraction interaction to lower the system energy. Therefore, the critical fluctuation effect will strengthen the depletion adsorption phenomena. Obviously, the critical depletion phenomena will be strengthened by a highly confining geometry. For case of the spherical cavity, a smaller radius will strengthen the critical depletion adsorption than a larger radius does. In addition, it is obvious that an attractive surface will strengthen the accumulation and a repulsive surface will strengthen the depletion, one can easily explain this conclusion from the point of view of energy.

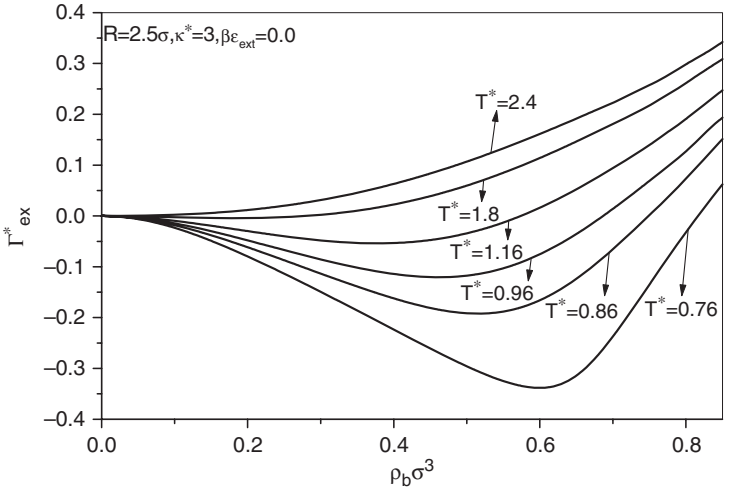

Figure 9. Influence of temperature on the $\Gamma^*_{ex} - \rho_b\sigma^3$ curve for the hard spherical cavity of radius $R = 2.5\sigma$, the potential range parameter $\kappa^* = 3$.

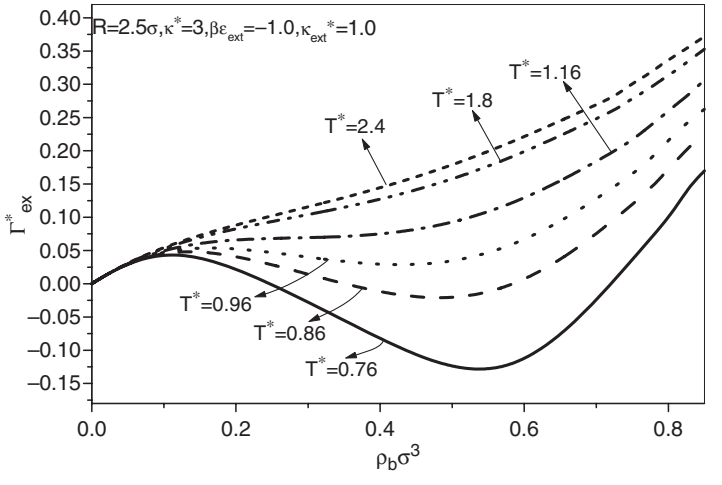

Figure 10. Influence of temperature on the $\Gamma^*_{ex} - \rho_b\sigma^3$ curve for the attractive spherical cavity of radius $R = 2.5\sigma$, the potential range parameter $\kappa^* = 3$ and the external potential parameters are shown in the figure.

With the above mechanism, one can explain the calculated results in Figures (5–12). Figure 5 surely displays the critical depletion adsorption around the critical region, but how to explain why the minimum Γ^*_{ex} occurs at a coexistence bulk density larger than the respective critical density? It is well known that the critical density is intermediate, as explained earlier, at the intermediate density region and that the critical depletion adsorption can be strengthened by an increase of the density.

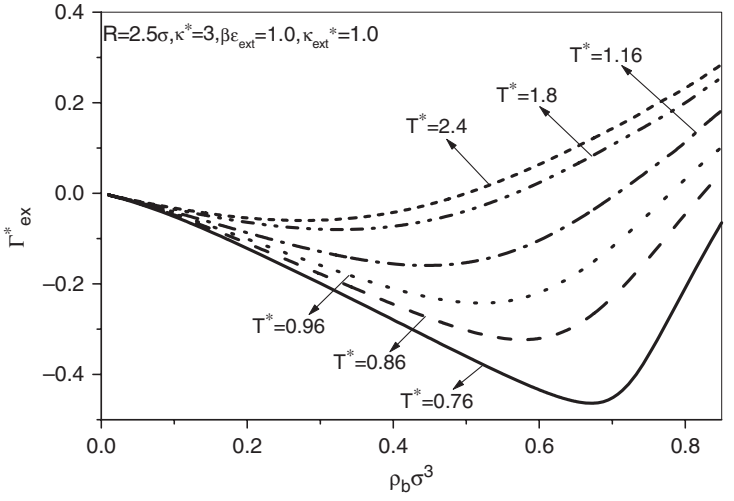

Figure 11. Influence of temperature on the $\Gamma^*_{ex} - \rho_b\sigma^3$ curve for the repulsive spherical cavity of radius $R = 2.5\sigma$, the potential range parameter $\kappa^* = 3$ and the external potential parameters are shown in the figure.

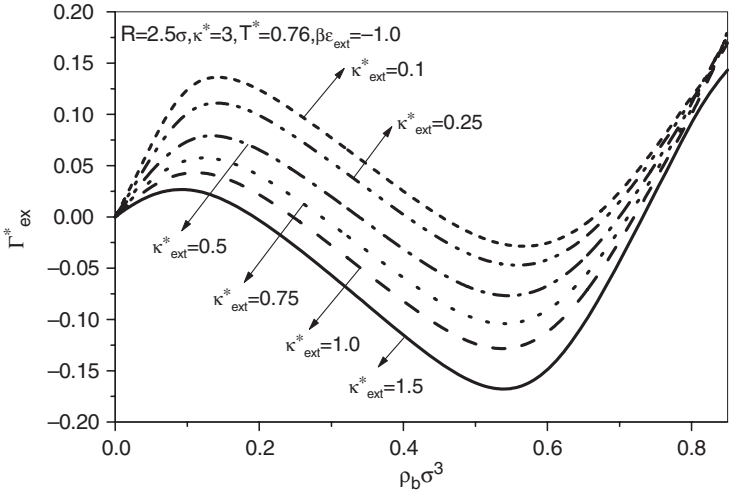

Figure 12. Influence of external potential range parameter κ^*_{ext} on the $\Gamma^*_{ex} - \rho_b\sigma^3$ curve for an attractive spherical cavity of radius $R = 2.5\sigma$. Note: The potential range parameter $\kappa^* = 3$, and the temperature is fixed at $T^* = 0.76$.

Figure 6(a) describes the influence of the geometrical size on the depletion adsorption. According to the above mechanism, the smallest geometrical size $R = 2.5\sigma$ should correspond to the strongest depletion, but the calculated results in Figure 6(a) seem to contradict the qualitative analysis since Figure 6(a) shows that $R = 2.5\sigma$ corresponds to the smallest depletion. Considering that the value of Γ^*_{ex} also depends on the surface area per volume, therefore Γ^*_{ex} is not an appropriate quantity

for describing singly the depletion effect for which the appropriate quantity should be the excess average density ρ_{ex-ave} in the spherical cavity given by

$$\rho_{ex-ave} = \int_0^R [\rho(\mathbf{r}) - \rho_b]d\mathbf{r}/(4\pi R^3/3). \quad (24)$$

In Figure 6(b) ρ_{ex-ave} as a function of the coexistence bulk density is presented for the same parameter set as in Figure 6(a), one clearly observes that the curve for $R = 2.5\sigma$ moves to the lowest position in agreement with the above qualitative analysis. Correspondingly, the curves for $R = 3.5\sigma$, 4.5σ move up to higher positions in sequence. How to explain the observation that the coexistence bulk density corresponding to the minimum $\rho_{ex-ave}\sigma^3$ increases when the geometrical size R decreases? As the geometrical size R decreases, the critical depletion is strengthened according to the above mechanism, thus a higher coexistence bulk density is required to restrain the depletion adsorption.

Figures 7 and 8, respectively, describe the influences of the attractive and repulsive external fields on the critical depletion phenomena. Obviously, the attractive external field offsets the critical fluctuation effect and therefore raises Γ^*_{ex}. On the contrary, the repulsive external field strengthens the critical fluctuation effect and therefore lowers Γ^*_{ex}. The larger the attractive external field or the repulsive external field strength is, the more significant the offsetting or strengthening is. The influences of temperature on the critical depletion phenomena for neutral, attractive and repulsive external fields are respectively described in Figures (9–11), which shows that the more away from the critical temperature, the more significant the depletion phenomena is restrained. From Figures (7–11), one general phenomena can be found, which indicates that the coexistence bulk densities corresponding to the largest depletion adsorption (i.e. the smallest Γ^*_{ex} or $\rho_{ex-ave}\sigma^3$) move to a higher value as the depletion phenomena is strengthened. This can be explained by the same mechanism, which explains the Figure 6(b).

Influence of the range parameter κ^*_{ext} of the attractive external field on the $\Gamma^*_{ex} - \rho_b\sigma^3$ curve is presented in Figure 12 for the parameter combinations as shown in the figure. It is shown that as the range parameter κ^*_{ext} increases, the external field becomes less attractive, consequently the $\Gamma^*_{ex} - \rho_b\sigma^3$ curve moves to a lower position in the figure. What remains to be explained in detail is why the coexistence bulk density corresponding to the minimum Γ^*_{ex} moves to a smaller value as the depletion adsorption is strengthened by a high κ^*_{ext}, since this observation contradicts with the above analysis. We will explain this 'unusual phenomena' as follows. Obviously, the depletion adsorption can occur more easily for a high κ^*_{ext} value than for a low κ^*_{ext} value. Thus, for the high κ^*_{ext} case, it is not the most effective route to resort to the intermediate density-strengthening depletion mechanism to increase the depletion, since this mechanism will also incur counter-depletion effect as it will lead to a large deviation from the critical point. It is the interaction between the two counter effects, which leads to a faster arrival at the minimum Γ^*_{ex} point for the high κ^*_{ext} case than for the low κ^*_{ext} case.

4. Conclusions

This article reports that the accuracy of the non-uniform fifth-order TPT [14d] for the density profiles of the HCAY fluid confined in a spherical cavity is generally

higher than the third-order + second-order perturbation DFT [9a]. Considering that the non-uniform fifth-order TPT is based on several ansatzs for the bulk second-order DCF, its reliability for other model potentials, particularly for those effective interaction potentials, which are of complicated mathematical forms, is worth further separate investigations. Extensive investigation about the adsorption in critical region is carried out, we find the interesting critical depletion adsorption phenomena whose physical explanation is in agreement with the theoretically calculated results. The critical depletion adsorption will influence the effective potential [27] between the colloidal particles, and certainly will also influence the phase behaviour [28] of complex fluids. All of these problems will be investigated in future research.

Acknowledgements

This project was supported by Postdoctoral Science Foundation of Central South University, China.

References

[1] D. Henderson, *Fundamentals of Inhomogeneous Fluids* (Marcel Dekker, New York, 1992).
[2] (a) F. van Swol and J.R. Henderson, Phys. Rev. A **40**, 2567 (1989); (b) F. van Swol and J.R. Henderson, Phys. Rev. A **43**, 2932 (1991).
[3] (a) P. Tarazona, Phys. Rev. A **31**, 2672 (1985); (b) W.A. Curtin and N.W. Ashcroft, *ibid.* **32**, 2909 (1985).
[4] (a) Y. Rosenfeld, Phys. Rev. Lett. **63**, 980 (1989); (b) E. Kierlik and M.L. Rosinberg, Phys. Rev. A **42**, 3382 (1990).
[5] (a) S. Zhou, New J. Phys. **4**, 36 (2002); (b) S. Zhou, Phys. Lett. A **319**, 279 (2003); (c) S. Zhou, Chem. Phys. **297**, 171 (2004); (d) **289**, 309 (2003); (e) S. Zhou, J. Phys. Chem. B **108**, 3017 (2004); (f) **106**, 7674 (2002).
[6] (a) S. Zhou and E. Ruckenstein, J. Chem. Phys. **112**, 8079 (2000); (b) S. Zhou, *ibid.* **113**, 8719 (2000); S. Zhou and E. Ruckenstein, *ibid.* **112**, 5242 (2000); (c) S. Zhou, Phys. Rev. E **63**, 061206 (2001); (d) **63**, 051203 (2001); (e) S. Zhou and X. Zhang, *ibid.* **64**, 011112 (2001); (f) S. Zhou, J. Chem. Phys. **115**, 2212 (2001); (g) S. Zhou, J. Phys. Chem. B **105**, 10360 (2001).
[7] (a) V.C. Weiss, J. Chem. Phys. **125**, 084718 (2006); (b) A. Mejía and L.F. Vega, *ibid.* **124**, 244505 (2006); (c) B. Husowitz and V. Talanquer, *ibid.* **126**, 224703 (2007).
[8] (a) H.H. von Grünberg and R. Klein, J. Chem. Phys. **110**, 5421 (1999); (b) X.C. Zeng and D.W. Oxtoby, *ibid.* **93**, 2692 (1990); (c) D.W. Marr and A.P. Gast, *ibid.* **99**, 2024 (1993).
[9] (a) S. Zhou, Commun. Theor. Phys. **40**, 721 (2003); (b) S. Zhou, Phys. Rev. E **68**, 061201 (2003); (c) S. Zhou, J. Chem. Phys. **121**, 895 (2004); (d) S. Zhou, J. Phys. Chem. B **109**, 7522 (2005).
[10] (a) S. Zhou, J. Chem. Phys. **124**, 144501 (2006); (b) S. Zhou, Int. J. Mod. Phys. B **20**, 469 (2006); (c) S. Zhou, Mol. Simul. **32**, 1165 (2006).
[11] (a) G. Tellez and E. Trizac, Phys. Rev. E **68**, 061401 (2003); (b) C.N. Patra and S.K. Ghosh, *ibid.* **49**, 2826 (1994); (c) C.N. Patra and S.K. Ghosh, J. Chem. Phys. **100**, 5219 (1994); (d) O. Pizio and S. Sokolowski, J. Chem. Phys. **125**, 024512 (2006).
[12] A. Kol and B.B. Laird, Mol. Phys. **90**, 951 (1997).
[13] (a) M.B. Sweatman, Phys. Rev. E **63**, 031102 (2001); (b) S.-C. Kim and S.H. Lee, J. Phys. Condens. Matter **16**, 6365 (2004).

[14] (a) S. Zhou, Phys. Rev. E **74**, 031119 (2006); (b) S. Zhou, J. Chem. Phys. **125**, 144518 (2006); (c) S. Zhou, J. Phys. Chem. B **111**, 10736 (2007); (d) S. Zhou, Phys. Rev. E **77**, 041110 (2008); (e) S. Zhou and J.R. Solana, Chem. Rev. **109**, 2829 (2009); (f) S. Zhou, Phys. Rev. E **79**, 011126 (2009); (g) S. Zhou, J. Chem. Phys. **131**, 134702 (2009); (h) S. Zhou, Theor. Chim. Acta **124**, 279 (2009).
[15] N.F. Carnhan and K.E. Starling, J. Chem. Phys. **51**, 635 (1969).
[16] (a) J.A. Barker and D. Henderson, J. Chem. Phys. **47**, 2856 (1967); (b) J.A. Barker and D. Henderson, Rev. Mod. Phys. **48**, 587 (1976).
[17] (a) E. Thiele, J. Chem. Phys. **39**, 474 (1963); (b) M.S. Wertheim, Phys. Rev. Lett. **19**, 321 (1963).
[18] S. Zhou, J. Chem. Phys. **110**, 2140 (1999).
[19] S. Zhou and A. Jamnik, J. Chem. Phys. **122**, 064503 (2005).
[20] S. Zhou, Chem. Phys. **310**, 129 (2005).
[21] J.R. Henderson, in *Fundamentals of Inhomogeneous Fluids*, edited by D. Henderson (Marcel Dekker, New York, 1992), p. 23.
[22] (a) S. Zhou, J. Colloid Interface Sci. **298**, 31 (2006); (b) S. Zhou, Phys. Rev. E **74**, 011402 (2006).
[23] J.K. Percus, in *The Equilibrium Theory of Classical Fluids*, edited by H.L. Frisch and A.L. Lebowitz (Benjamin, New York, 1964), p. 113.
[24] K.P. Shukla, J. Chem. Phys. **112**, 10358 (2000).
[25] S. Zhou and A. Jamnik, Phys. Rev. E **73**, 011202 (2006); S. Zhou and A. Jamnik, J. Phys. Chem. B **110**, 6924 (2006).
[26] Y. Tang and J. Wu, Phys. Rev. **E 70**, 011201 (2004).
[27] (a) T. Araki and H. Tanaka, Phys. Rev. E **73**, 061506 (2006); (b) S. Zhou, Chem. Phys. Lett. **392**, 110 (2004); (c) **399**, 323 (2004); (d) **399**, 315 (2004); (e) S. Zhou, J. Colloid Interface Sci. **288**, 308 (2005).
[28] (a) F.L. Verso, R.L.C. Vink, D. Pini and L. Reatto, Phys. Rev. E **73**, 061407 (2006); (b) A. Fortini, M. Schmidt, M. Dijkstra, *ibid*. **73**, 051502 (2006); (c) S. Zhou, J. Phys. Chem. B **113**, 8635 (2009); (d) J. Chem. Phys. **130**, 014502 (2009); (e) **128**, 104511 (2008); (f) **127**, 084512 (2007).